

Systematic study of low-energy incomplete fusion: Role of entrance channel parametersAbhishek Yadav,^{1,*} Pushpendra P. Singh,² Mohd. Shuaib,³ Vijay R. Sharma,¹ Indu Bala,¹ Unnati,⁴ Sunita Gupta,⁵ D. P. Singh,⁶ M. K. Sharma,⁷ R. Kumar,¹ S. Murlithar,¹ R. P. Singh,¹ B. P. Singh,³ and R. Prasad³¹*Nuclear Physics Group, Inter-University Accelerator Centre, New Delhi 110 067, Delhi, India*²*Physics Department, Indian Institute of Technology Ropar, Roopnagar 140 001, Panjab, India*³*Physics Department, Aligarh Muslim University, Aligarh 202 002, Uttar Pradesh, India*⁴*Department of Physics & Astrophysics, Delhi University, New Delhi 110 007, Delhi, India*⁵*Physics Department, Agra College, Agra 282 001, Uttar Pradesh, India*⁶*Department of Physics, University of Petroleum and Energy Studies, Dehradun 248 007, Uttarakhand, India*⁷*Physics Department, S. V. College, Aligarh 202 001, Uttar Pradesh, India*

(Received 15 July 2017; published 18 October 2017)

An attempt has been made to investigate the role of various entrance channel parameters in low-energy ($\approx 4\text{--}7$ MeV/nucleon) incomplete fusion reactions through excitation function measurements. The analysis of measured excitation functions, in the framework of statistical model code PACE4, reveals that the xn/pxn channels are populated, predominantly, via complete fusion processes. However, in the production of α -emitting channels, even after correcting for the precursor decay contribution, a significant enhancement as compared to statistical model predictions has been observed, which may be attributed due to the contribution of breakup processes. The observed enhancement is found to increase with projectile energy. Further, the comparison of present work with literature data reveals the dependence of incomplete fusion on mass-asymmetry of interacting partners, α - Q value of the projectile, and also on $Z_P Z_T$ (the Coulomb factor). From the present analysis, it may be concluded that a single entrance channel parameter (i.e., mass asymmetry or $Z_P Z_T$ or α - Q value) is not able to explain, completely, the yields of the low-energy incomplete fusion component. Therefore, a combination of these parameters and/or a parameter which can incorporate all gross features of interacting partners should be chosen to get a systematics for such reactions.

DOI: [10.1103/PhysRevC.96.044614](https://doi.org/10.1103/PhysRevC.96.044614)**I. INTRODUCTION**

Fusion reactions induced by heavy ions (HIs) play an important role in nuclear physics, since they enable us to study the properties of nuclei even away from the stability line [1–4]. As a result, a comprehensive understanding of the reaction mechanism involved in HI-induced reactions has always been an active area of investigation [5–10]. During the last couple of decades, the significant contribution of the incomplete fusion (ICF) reactions to the HI-reaction mechanism has been observed at energies in the vicinity of Coulomb barrier (V_b), where complete fusion (CF) is one of the dominant process [10–16]. The CF reactions correspond to the complete amalgamation of the projectile and the target nuclei, wherein the collision enters into the region of an attractive potential for input angular momentum $\ell < \ell_{\text{crit}}$. However, in case of ICF reactions the fusion pocket disappears in the effective potential energy curve with partial waves $\ell > \ell_{\text{crit}}$ (for peripheral interactions and/or at high beam energies) [17]. Hence the projectile may break up into its constituents to provide sustainable input angular momentum. Consequently, one of the fragments may fuse with the target nucleus, forming a composite system with reduced excitation energy and mass, while the remnant flows in the forward direction almost with the beam velocity. Some signatures of the ICF reactions are (i) higher production yields over the statistical model predic-

tions, particularly for α -emitting channels [14], (ii) fractional linear momentum transfer from the projectile to the target nucleus [15,16], (iii) entirely distinct deexcitation patterns of CF and ICF residues [10], and (iv) broader angular distributions for ICF residues than for the CF events [15].

In order to understand the observation of fast α particles in the exit channel [18,19], several attempts have been made [20–30]. A brief description of some of these models is given elsewhere [14]. Some of the most widely employed models to explain ICF data are the breakup fusion model [20,21], sum-rule model [22], exciton model [23], promptly emitted particles model [24], and overlap model [25–28]. These models have, generally, been used to fit the experimental data obtained at energies $E \geq 10$ MeV/nucleon or so. At still higher energies (≥ 20 MeV/nucleon) the experimental data may be explained, to some extent, by including the contributions of projectile breakup and/or nucleon coalescence. But no satisfactory explanation of ICF data could be made at low energies (i.e., 4–7 MeV/nucleon), because of the unavailability of any reliable theoretical model and/or systematics. This triggered a renewed interest in investigating the dynamics of low-energy breakup reactions.

During the last couple of decades, the presence of low-energy ICF reactions and their dependence on various entrance channel parameters have been studied. Morgenstern *et al.* has correlated the ICF fraction, the contribution of ICF to total fusion cross section, with entrance channel mass asymmetry at relatively higher energies ≥ 10 MeV/nucleon [31], where ICF is found to depend upon the entrance channel mass

* abhishekyadav117@gmail.com

asymmetry $\mu = A_T/(A_T + A_P)$ of interacting partners, where A_P and A_T are the atomic mass numbers of the projectile and target nuclei, respectively. Apart from mass asymmetry, Singh *et al.* has introduced the projectile-dependent mass-asymmetry systematics at low energies [32]. Further, the importance of projectile structure has been explained in one of our recent papers using the projectile's α - Q value (the energy required to separate an α particle from the projectile), which states that a larger negative Q_α value of the projectile will lead to a smaller breakup probability of the projectile [33]. Principally, the above discussed observations are somewhat conditional in nature; i.e., they are obtained by fixing either the projectile or the target nuclei. Recently, an attempt was made by Shuaib *et al.* [34] to find out some systematics for several projectile-target combinations. They plotted the ICF fraction for ^{12}C , ^{16}O , and ^{19}F projectiles with different targets ($Z_P Z_T \approx 270$ – 640 ; 11 projectile-target combinations), where a linear dependence between ICF fraction and $Z_P Z_T$ for these systems has been observed. However, it is worthwhile to notice that the proposed $Z_P Z_T$ systematics [34] is unable to explain the data for systems with same $Z_P Z_T$ values, e.g., projectile isotopes on the same target nuclei (e.g., $^{12,13}\text{C} + X$, $^{16,18}\text{O} + X$) or the same projectile with different target isotopes (e.g., $x + ^{144,154}\text{Sm}$). Therefore, the pending question of ICF dependence on entrance channel parameters has developed interest in looking for the general systematics for low-energy ICF reactions. In the present work, with a motivation to understand the dependence of ICF reactions on entrance channel parameters in a comprehensive way, the excitation functions (EFs) of reaction residues populated in $^{13}\text{C} + ^{159}\text{Tb}$ interactions at several beam energies, ranging from $\approx 1.01V_b$ to $1.68V_b$ (V_b being the Coulomb barrier), have been measured and analyzed within the framework of a statistical model code [35,36]. The present analysis includes a large number of projectile-target combinations ($Z_P Z_T \approx 240$ – 670 ; 21 projectile-target combinations) to investigate all possible aspects of low-energy ICF reactions. The present paper is organized as follows: A brief description of the experimental methodology is given in Sec. II, while Sec. III deals with the details of the measurements, results, and their interpretation, and finally the summary is presented in Sec. IV.

II. EXPERIMENTAL DETAILS

The experiments were planned and performed at the Inter-University Accelerator Centre (IUAC), New Delhi, India using ^{13}C (non- α -clustered) beam with ^{159}Tb target. The activation technique followed by offline γ -ray spectroscopy was employed. Isotopically pure ^{159}Tb targets (target thickness $t_m \approx 1.2$ – 2.5 mg/cm²) and aluminum catcher/energy-degrader foils ($t_m \approx 1.5$ – 2.5 mg/cm²) were prepared by rolling technique, and the uniformity of each target was verified by α -transmission method. In order to achieve a wide energy range in the allotted beam time, the energy-degradation technique was used; i.e., each target foil was backed by an Al catcher foil (hereafter called the target-catcher foil assembly). Placing the Al catcher foil as backing of the target fulfilled two purposes: (i) stopping the recoiling products produced during the irradiations in their respective target-catcher assembly,

and (ii) degrading the beam energy. In this experiment, six stacks (each made by three target-catcher foil assemblies) were prepared and irradiated at different beam energies: ≈ 58 , 60, 70, 73, 85, and 88 MeV. The irradiations were carried out in the General Purpose Scattering Chamber (GPSC) which has an in-vacuum transfer facility, used to minimize the lapse time between the stop of the irradiation and the beginning of the counting of the activity induced in a target-catcher assembly [37]. Considering the half-lives of interest, the irradiations were carried out for 8–10 h duration for each stack. A Faraday cup was installed behind the target-catcher foil assembly to monitor the beam current, ≈ 25 – 30 nA, during all the irradiations. The incident beam energy on each target foil in a stack has been estimated using the code SRIM [38]. For example, at the highest incident energy (i.e., 87.62 MeV), the uncertainty in the energy is estimated to be ± 0.38 MeV, and, at the lowest incident energy (i.e., 52.47 MeV) it is estimated to be ± 0.85 MeV.

The radioactivity produced in the target-catcher foil assemblies was recorded, separately, at several time intervals by a precalibrated, high-resolution, high-purity germanium (HPGe) detector coupled to a computer-automated measurement and control (CAMAC) based data acquisition system [39]. The HPGe detector used in this experiment was calibrated using standard γ sources, e.g., ^{60}Co and ^{152}Eu . The efficiency of the detector was determined using the standard γ -ray sources at various source-detector separations to wash out the solid-angle effect. The energy resolution of the detector was estimated to be 2.0 keV for the 1.33 MeV γ line of the ^{60}Co source. A 50 Hz pulser was used to determine the dead time of the detector.

III. ANALYSIS: RESULTS AND THEIR INTERPRETATION

The analysis of data was carried out first with the measurement of cross-sections of residues, populated during the projectile-target interactions, at each studied energy; i.e., the EFs were measured and then compared with the predictions of a statistical model code to understand the involved reaction mechanism. In order to measure the EFs, the reaction residues were identified in the recorded γ -ray spectra by their characteristic γ lines, which were further confirmed by studying their decay curves. As a representative case, a typical γ -ray spectrum obtained at incident energy 87.62 ± 0.38 MeV is shown in Fig. 1, where some of the γ peaks corresponding to different reaction products, produced during the projectile-target interactions, are also labeled. In the inset of this figure, as a typical example, the decay curve of ^{168}Lu ($t_{1/2} = 5.5$ min) residues is shown; it is in agreement with the literature value of its half-life and confirms its identification. The identified reaction residues are tabulated in Table I, with their spectroscopic properties taken from Refs. [40,41]. Not all the γ lines in the spectrum could be assigned to the characteristic γ lines of CF and ICF residues. The origin of those γ lines could be other reaction processes, such as fusion-fission of the completely and/or incompletely fused composite system [42]. Further, the standard formulation was used to determine the production cross sections of reaction products [14]. Usually a reaction residue may be populated via a specific channel in its excited

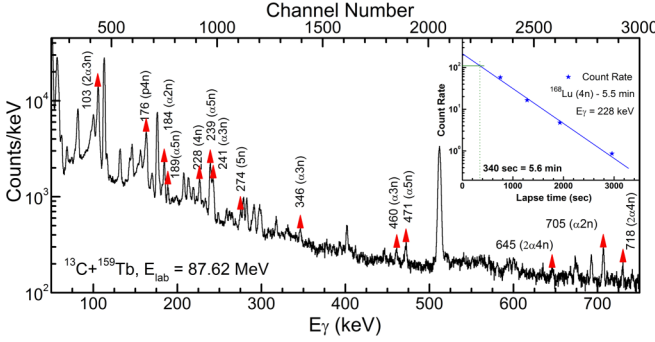


FIG. 1. A typical γ -ray spectrum obtained at 87.62 ± 0.38 MeV beam energy in $^{13}\text{C} + ^{159}\text{Tb}$ interactions. Some of the identified γ lines corresponding to different CF and/or ICF residues are labeled. The inset of this figure shows the decay curve of ^{168}Lu ($t_{1/2} = 5.5$ min) residues populated via the $4n$ channel.

state and often deexcite by emitting several γ rays of different energies. Therefore, the reported values of the cross sections for some residues are the weighted averages of cross sections obtained for their different γ rays [43]. Hence, in the present work, the EFs of radionuclides $^{169}\text{Lu}(3n)$, $^{168}\text{Lu}^{g+m}(4n)$, $^{167}\text{Lu}(5n)$, $^{167}\text{Yb}(p4n)$, $^{166}\text{Tm}(\alpha 2n)$, $^{165}\text{Tm}(\alpha 3n)$, $^{163}\text{Tm}(\alpha 5n)$, $^{162}\text{Ho}^m(2\alpha 2n)$, $^{161}\text{Ho}(2\alpha 3n)$, $^{160}\text{Ho}^g(2\alpha 4n)$, and $^{160}\text{Ho}^m(2\alpha 4n)$, populated in the interactions of the $^{13}\text{C} + ^{159}\text{Tb}$ system, have been measured.

TABLE I. List of identified reaction residues, for which EFs have been measured, along with their spectroscopic properties.

Residue	$T_{1/2}$	J^π	E_γ (keV)	I^γ (%)
$^{169}\text{Lu}(3n)$	34.06 h	$7/2^+$	191.21	20.7
			960.62	23.5
$^{168}\text{Lu}^{g+m}(4n)$	5.5 min	3^+	198.86	180.0 ^a
			228.58	70.0 ^a
$^{167}\text{Lu}(5n)$	51.5 min	$7/2^+$	213.21	3.5
$^{167}\text{Yb}(p4n)$	17.5 min	$5/2^-$	113.34	55
			176.24	20.4
			705.31	10.4
$^{166}\text{Tm}(\alpha 2n)$	7.70 h	2^+	184.41	15.8
			296.03	23
$^{165}\text{Tm}(\alpha 3n)$	30.06 h	$1/2^+$	346.75	3.9
			460.14	3.0
			242.85	35
$^{163}\text{Tm}(\alpha 5n)$	1.81 h	$1/2^+$	296.03	23
			190.07	1.28
			239.67	4.1
$^{162}\text{Ho}^m(2\alpha 2n)$	1.12 h	1^+	471.29	3.8
			185.01	29.3
			282.73	11.5
$^{161}\text{Ho}(2\alpha 3n)$	2.48 h	$7/2^-$	103.03	3.6
$^{160}\text{Ho}^g(2\alpha 4n)$	25.6 min	5^+	197.03	14.0
			645.25	16.20
			197.03	14.0
			645.25	16.20
			728.18	30.8
$^{160}\text{Ho}^m(2\alpha 4n)$	5.02 h	2^-	879.39	20.2
			728.18	30.8

^aThese intensities are relative.

It is worthwhile to mention that the errors in the measured production cross sections may arise due to various sources, such as the nonuniformity of target foils, fluctuations in the beam current, the uncertainty in geometry-dependent efficiency of the HPGe detector, finite dead time of the spectrometer, etc. A detailed discussion on the error analysis is given elsewhere [14]. Attempts were made to minimize the uncertainties due to all the above factors, and the overall error including statistical errors is estimated to be $\leq 15\%$.

Further, to study the involvement of different reaction processes, the experimentally measured EFs were analyzed within the framework of the statistical model code PACE4 [35,36], which is based on the Hauser-Feshbach theory of CN decay [44]. The details of the code are given in Refs. [14,35,36]. In brief, this code uses the statistical approach of CN deexcitation by a Monte Carlo procedure. The angular momentum projections are calculated at each stage of deexcitation, which enables the determination of angular distribution of the emitted particles, and angular momentum conservation is explicitly taken into account. In this code, Gilbert and Cameron's nuclear level density parameter and spin cutoff parameter were adopted for the calculations [45]. This code has been modified to take into account the excitation energy dependence of level density parameter using the prescription of Kataria *et al.* [46]. The Bass model is used to calculate the CF cross sections [47]. In this code, the level density parameter ($a = A/K$ MeV $^{-1}$, where A is the mass number of the nucleus and K is a free adjustable parameter) is one of the important parameters. The value of free parameter K can be varied, within the physically justified limits [45], to reproduce the experimentally measured EFs.

A. xn/pxn channels: Calibration of the statistical model code

As has already been stated, the comparison of experimentally measured and theoretically predicted EFs may provide a method to understand the involved reaction mechanism in the production of reaction residues. Hence, the right choice of the parameters used in theoretical predictions through the statistical model code is a requisite step for the analysis. The experimentally measured EFs of ^{169}Lu , $^{168}\text{Lu}^{g+m}$, ^{167}Lu , and ^{167}Yb evaporation residues expected to be populated respectively via $3n$, $4n$, $5n$, and $p4n$ emission from the excited $^{172}\text{Lu}^*$ nucleus have been plotted in Fig. 2. During the decay-curve analysis, the evaporation residue $^{167}\text{Yb}(p4n)$, half-life 17.5 min, was found to be strongly fed from its higher charge isobar ("precursor" hereafter) $^{167}\text{Lu}(5n)$, having half-life 51.5 min, through β^+ emission. Notice that the half-life of the precursor (i.e., ^{167}Lu) is larger than the half-life of the daughter nuclei (i.e., ^{167}Yb). Hence, the independent production cross section (σ_{ind}) of ^{167}Yb has been deduced using the following successive radioactive decay formulation based on the Bateman equation [48]:

$$N_d(t) = C_{t=0} e^{-\lambda_d t} + \frac{P_{\text{pre}} \lambda_{\text{pre}}}{(\lambda_d - \lambda_{\text{pre}})} N_{\text{pre}}(t) e^{-\lambda_{\text{pre}} t} \quad (1)$$

In Eq. (1), $N_d(t)$ and $N_{\text{pre}}(t)$ are the numbers of daughter and precursor nuclei produced at any time t . $C_{t=0}$ is the cumulative (precursor + daughter) number of nuclei produced at the end

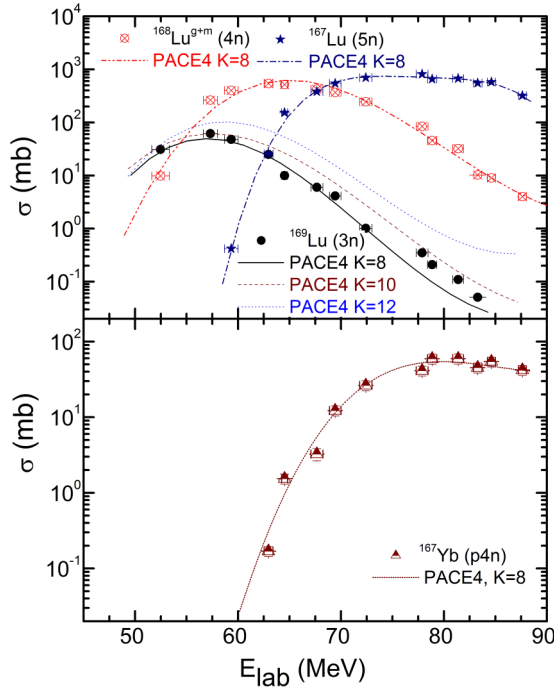


FIG. 2. Experimentally measured EFs of $^{169}\text{Lu}(3n)$, $^{168}\text{Lu}^{g+m}(4n)$, $^{167}\text{Lu}(5n)$, and $^{167}\text{Yb}(p4n)$ residues populated in the $^{13}\text{C} + ^{159}\text{Tb}$ system. The lines through the data points are predictions done using the PACE4 code (for details see text).

of the irradiation of the target. λ_{pre} and λ_d are the decay constants of precursor and daughter nuclei, respectively. P_{pre} is the branching ratio of the precursor decay to the final nucleus. The value of $N_{\text{pre}}(t)$ has been deduced from the experimentally measured decay curve of precursor ^{167}Lu . The number of independently produced daughter nuclei, $N_d(t)$ (^{167}Yb), at time t has been obtained by solving Eq. (1), which has been translated to the independent production cross section (σ_{ind}) of $^{167}\text{Yb}^{(\text{ind})}(p4n)$ and is plotted in Fig. 2 (lower panel). However, the EFs for other pxn channels could not be measured in the present work due to their short/long half-lives.

In order to study the production mechanism of reaction products formed via xn/pxn channels, an attempt has been made to reproduce the experimentally measured EFs of these channels using the statistical model code PACE4. The level density $a (=A/K \text{ MeV}^{-1})$ was varied by using different values of free parameter K . According to Gilbert and Cameron's level density systematics, values of the free parameter K significantly higher than $K = 10$ are unlikely for the excitation energy and mass region of interest. Nevertheless, in the present calculations K higher than 10 have been used to better elucidate the dependence of the calculated excitation functions on this parameter. Figure 2 shows the experimental EFs of xn/pxn channels compared with PACE4 predictions; notations are self-explanatory. As shown in this figure, the experimentally measured EFs for these channels are nicely reproduced by PACE4 predictions for the level density $a = A/8 \text{ MeV}^{-1}$, indicating the production of these residues through the deexcitation of a fully equilibrated compound nucleus ($^{172}\text{Lu}^*$) formed via complete fusion of ^{13}C with ^{159}Tb

target nuclei. Thus, the choice of parameters used for the analysis is suitable, and therefore the value of level density $a = A/8 \text{ MeV}^{-1}$ can be used consistently as a fixed parameter for the analysis of all the channels expected to be populated via both CF and ICF reaction processes.

B. α -emitting channels: Enhancement over PACE predictions

The EFs of seven α -emitting channels, $^{166}\text{Tm}(\alpha 2n)$, $^{165}\text{Tm}(\alpha 3n)$, $^{163}\text{Tm}(\alpha 5n)$, $^{162}\text{Ho}^m(2\alpha 2n)$, $^{161}\text{Ho}(2\alpha 3n)$, $^{160}\text{Ho}^g(2\alpha 4n)$, and $^{160}\text{Ho}^m(2\alpha 4n)$, populated through $^{13}\text{C} + ^{159}\text{Tb}$ interactions in the energy range $1.01V_b$ to $1.68V_b$, have been plotted in Fig. 3. Note that it is possible to explain all experimentally measured EFs with different choices of parameters of the statistical model code for individual channels, but from the physics point of view this is quite unreasonable. Therefore, in the present work all the calculations were performed consistently, using the same set of parameters for all the measured channels. It may be observed in Figs. 3(a)–3(f), that the experimentally measured EFs for all α -emitting channels are underpredicted by PACE4 calculations done with the same set of parameters as used to reproduce the EFs for xn and pxn channels. Solid blue curves are the PACE4 predictions for level density value $a = A/8 \text{ MeV}^{-1}$. It is worthwhile to mention that the code PACE4 does not take ICF into account; therefore, the experimentally observed higher production cross sections with respect to the theoretical predictions may be attributed to the ICF processes. Further, as can be noticed from Fig. 3, the ICF contribution is distributed over the full studied range of energy, and shows different energy dependence for different residues. Note that the residues populated via α -emitting channels may arise from CF and/or ICF processes. In the case of CF, the incident projectile (^{13}C) entirely fuses with the target nucleus (^{159}Tb) to form a fully equilibrated CN, which may eventually decay via an αxn channel. However, in the case of ICF, only a part of the incident projectile (i.e., $^{13}\text{C} \rightarrow ^9\text{Be} + \alpha$) fuses with the target nucleus to form an incompletely fused composite system, and the remnant α or ^9Be keeps on moving in the forward cone as a spectator. As a representative case, the residue ^{165}Tm can be populated in the following ways.

- (i) The CF of ^{13}C with ^{159}Tb : $^{13}\text{C} + ^{159}\text{Tb} \Rightarrow ^{172}\text{Lu}^* \Rightarrow ^{165}\text{Tm} + \alpha 3n$.
- (ii) When only a part of projectile ^{13}C (i.e., ^9Be) fuses with ^{159}Tb to form an incompletely fused composite system ($^{168}\text{Tm}^*$) while an α particle flows in the forward direction as a spectator. The excited $^{168}\text{Tm}^*$ may then decay via three neutrons ($3n$) as $^{13}\text{C}(^9\text{Be} + \alpha) \Rightarrow ^9\text{Be} + ^{159}\text{Tb} \Rightarrow ^{168}\text{Tm}^* \Rightarrow ^{165}\text{Tm} + 3n$ (α particle as a spectator).

Further, in order to deduce the ICF contribution in $\alpha xn/2\alpha xn$ channels, the same data reduction procedure has been used as that given in Ref. [14]. The contribution of ICF in the production of ^{166}Tm , ^{165}Tm , ^{163}Tm , $^{162}\text{Ho}^m$, ^{161}Ho , $^{160}\text{Ho}^g$, and $^{160}\text{Ho}^m$ residues has been deduced as $\Sigma\sigma_{ICF} = \Sigma\sigma_{\alpha xn+2\alpha xn}^{\text{exp}} - \Sigma\sigma_{\alpha xn+2\alpha xn}^{\text{PACE4}}$, by subtracting the PACE4 predictions for $\alpha xn + 2\alpha xn$ (done with the same set of parameters as for xn/pxn channels) from their corresponding experimentally measured excitation functions at each studied energy. Some

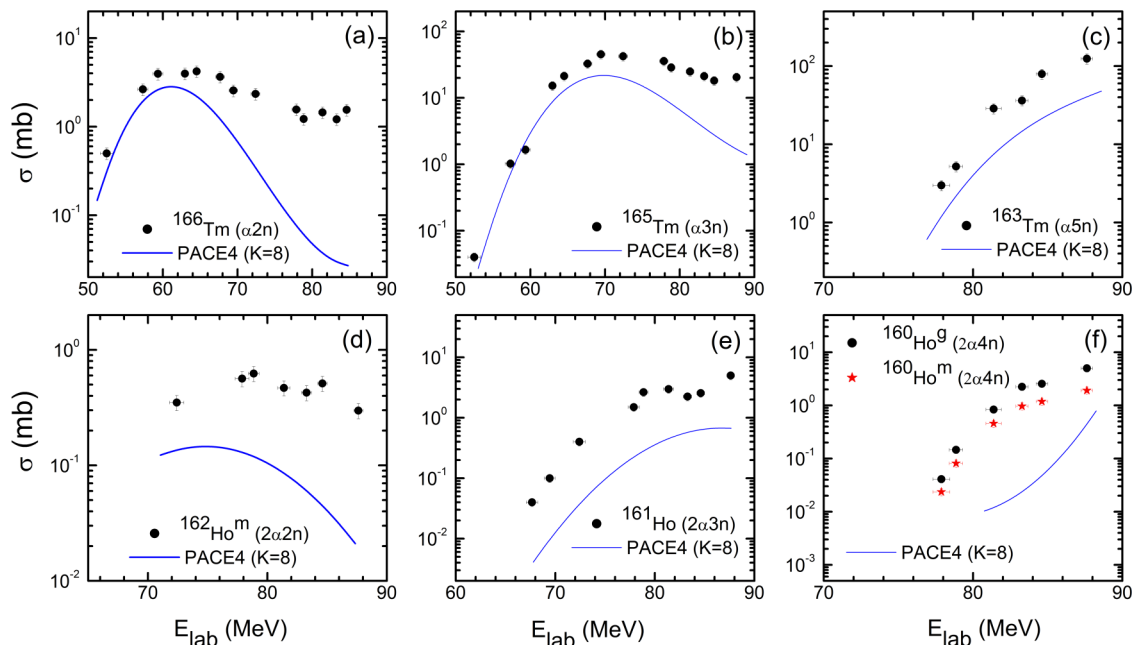


FIG. 3. Experimentally measured EFs of α -emitting channels are compared with the PACE4 predictions. Solid blue lines represent PACE4 predictions performed for $a = A/8 \text{ MeV}^{-1}$. See text for explanation.

recent reports [15,16] have indicated that the ICF contributions deduced using the above data reduction procedure have been found to be in good agreement with those obtained from the analysis of forward ranges and angular distributions of heavy recoils. It is of paramount importance to mention that the ICF contribution deduced from the recoil range distribution and angular distribution methods are independent of the statistical model predictions. This is because, in recoil range and angular distribution measurements, the CF and ICF contributions are deduced separately on the basis of full and partial linear momentum transfer events, respectively [15,16]. As already discussed, the αxn channels may be populated via both CF and ICF reaction processes; thus, in our previous measurements of recoil range and angular distributions [15,16], the CF contribution in the production of αxn channels are satisfactorily reproduced via PACE4 predictions done with the same set of parameters as used to calculate the cross sections of xn/pxn channels. This reproduction of CF contributions, in αxn channels, is a clear validation of the choice of PACE4 parameters. Here a good agreement between the data of two independent measurements puts confidence in the choice of PACE4 parameters, as well as the present method of deducing ICF contributions using PACE4 predictions.

C. ICF strength function and its sensitivity to entrance channel parameters

To compare the strengths of CF and ICF components, the ICF strength function (F_{ICF}) has been deduced for the present system. The F_{ICF} is a measure of strength of ICF relative to total fusion, and is defined as $F_{ICF} (\%) = (\Sigma\sigma_{ICF}/\sigma_{TF}) \times 100$, $\sigma_{TF} = \Sigma\sigma_{CF} + \Sigma\sigma_{ICF}$. In order to study the dependence of the reaction dynamics on the projectile type, the calculated values of F_{ICF} for the present system have been compared with

the strength functions for other systems in which different projectiles hit the same target ^{159}Tb , and these values are plotted in Fig. 4. In this figure the F_{ICF} values are plotted as a function of normalized beam energy, to wash out the effect of different Coulomb barriers. However, note that some of the reaction channels could not be measured due to their short or very long half-lives. In order to include the missing CF channels, the value of $\Sigma\sigma_{CF}$ has been corrected using the PACE4 predictions. However, no such correction could be applied for the ICF channels. This is because at present there is no established theoretical model or systematics available that may predict ICF contribution at such low energies. Therefore, the value of F_{ICF} in Fig. 4 may be taken as the lower limit of ICF for the system. The effect of various entrance channel

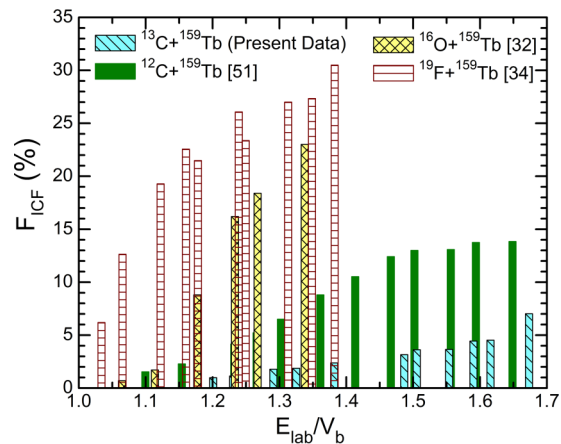


FIG. 4. The comparison of F_{ICF} values for different projectiles on same target ^{159}Tb . The x axis is normalized by their corresponding Coulomb barriers (for details see text).

parameters on ICF reaction dynamics will be discussed in the following subsections.

1. ICF sensitivity to the beam energy

As shown in Fig. 4, the value of F_{ICF} is found to be $\approx 1\%$ at $1.2V_b$ (i.e., 20% above the barrier), and increases smoothly up to $\approx 7\%$ at the highest measured energy (i.e., $1.68V_b$) for the $^{13}\text{C} + ^{159}\text{Tb}$ system. Similarly, the F_{ICF} for other systems are also found to increase with the increase in the incident energy. This is likely, as the increase in incident energy imparts larger angular momentum to the system, which leads to flattening of the fusion pocket in the effective potential energy curve. In order to restore the fusion pocket and, of course, to provide sustainable input angular momenta, the projectile breaks up into its constituents, leading to the ICF processes. As examples some of the breakup combinations observed in ^{16}O induced reactions, ^{16}O may break up into (i) ^{12}C and ^4He (α) clusters, (ii) ^8Be and ^8Be fragments, and/or (iii) four α particles. Depending on the favorability of input angular momentum conditions, one or a group of fragments may fuse with the target nucleus to form an incompletely fused composite system.

Further, notice in Fig. 4 that the values of F_{ICF} for ^{19}F (non- α -cluster) projectile are larger than the well-known α -clustered projectiles ^{16}O and ^{12}C , over the entire studied energy range. Also, the ^{13}C projectile has smaller ICF fraction than the other projectiles. It may also be observed in Fig. 4 that not only the magnitudes of F_{ICF} are different for different projectiles but the energy for the onset of ICF, for different systems, is also different. In case of ^{12}C , the onset of ICF (E_{th}^{ICF}) seems to take place at a relatively lower energy (i.e., $1.1V_b$) than for ^{13}C ($E_{th}^{ICF} = 1.2V_b$) induced reactions with ^{159}Tb target. For ^{19}F and ^{16}O projectiles the onset E_{th}^{ICF} is $1.02V_b$ and $1.06V_b$, respectively. Thus, ^{19}F , among all projectiles, has the smallest energy at which ICF starts. It follows from these observations that some property associated with the structure of the projectile (e.g., binding energy, Q_α value, shape of the nuclei, etc.), other than the cluster nature, also influences the ICF reaction dynamics.

2. ICF sensitivity to the mass asymmetry of interacting partners

In order to understand how ICF-fraction depends on the entrance channel mass asymmetry [$\mu = A_T/(A_T + A_P)$], the present data have also been analyzed within the framework of Morgenstern's mass-asymmetry systematics [31], according to which ICF reactions contribute significantly for more mass-asymmetric systems. Therefore, the values of F_{ICF} for the $^{13}\text{C} + ^{159}\text{Tb}$ system (present work) have been compared with those obtained for $^{12}\text{C} + ^{115}\text{In}$ [49], ^{159}Tb [50], ^{169}Tm [51], ^{181}Ta [52], ^{175}Lu [53]; $^{13}\text{C} + ^{169}\text{Tm}$ [54], ^{181}Ta [52]; $^{16}\text{O} + ^{93}\text{Nb}$ [55], ^{103}Rh [14], ^{115}In [56], ^{159}Tb [32], ^{165}Ho [57], ^{169}Tm [32]; $^{18}\text{O} + ^{159}\text{Tb}$ [58]; $^{19}\text{F} + ^{159}\text{Tb}$ [34], ^{169}Tm [59], ^{175}Lu [60]; and $^{20}\text{Ne} + ^{55}\text{Mn}$ [61], ^{59}Co [62], ^{165}Ho [63] systems at a constant normalized beam energy ($E_{lab}/V_b = 1.35$) as a function of entrance channel mass asymmetry, and are presented in Fig. 5. Note that for some projectiles the available data are limited to only a few target nuclei. From this figure it may be observed that the ICF strength function almost

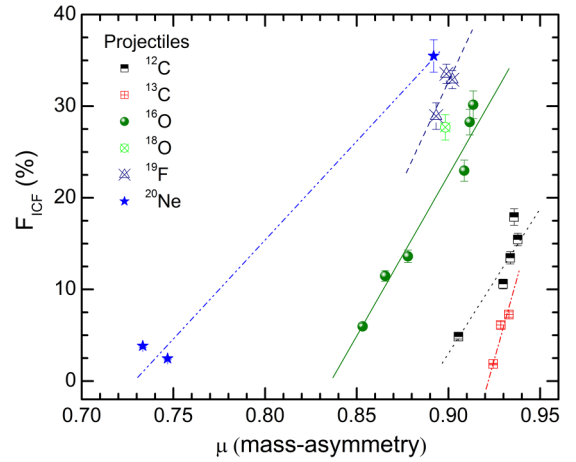


FIG. 5. The incomplete fusion fraction F_{ICF} for various systems are compared in terms of the mass asymmetry (μ) of the interacting partners at a constant E_{lab}/V_b value. The lines are linear fits to data, separately for each projectile (see text for explanation).

linearly increases, separately for each projectile, with the increase in their mass asymmetry. Figure 5 also shows that the magnitude of F_{ICF} for systems with the same mass asymmetry and different projectiles are very different; e.g., for systems $^{12}\text{C} + ^{115}\text{In}$ ($\mu = 0.9055$), $^{16}\text{O} + ^{159}\text{Tb}$ ($\mu = 0.9086$), and $^{19}\text{F} + ^{175}\text{Lu}$ ($\mu = 0.9021$), with almost same mass asymmetry, the values of F_{ICF} are $\approx 5\%$, 23% , and 33% , respectively. This is in contrast to the mass-asymmetry systematics [31], according to which the ICF depends only on the degree of mass asymmetry in the entrance channel. Another important observation from Fig. 5 is that the rates of rise of the magnitude of F_{ICF} are different for different projectiles. This clearly shows that the projectile structure, along with the mass asymmetry of the projectile-target pair, plays a role in ICF reactions at these low energies. Further, these results are in line with the projectile-dependent mass-asymmetry systematics presented by Singh *et al.* [32].

3. ICF sensitivity to the α - Q value of the projectile

The different magnitudes of ICF fraction for ^{19}F , ^{16}O , ^{13}C , and ^{12}C induced reactions presented in Fig. 4, as well as the observations discussed in the previous subsection based on Fig. 5, demonstrate the importance of projectile structure effect on low energy ICF reactions. The features revealed in Fig. 4 could not be explained on the basis of binding energies of the projectile, as the ^{19}F projectile (with more binding energy than ^{18}O or $^{12,13}\text{C}$) has a larger magnitude of incomplete fusion fraction. Further, note that ^{16}O and ^{12}C are well-known α -cluster nuclei with α - Q values Q_α of -7.16 and -7.37 MeV, respectively. The projectile's Q_α value is nothing but the energy required to separate an α particle from the projectile. ^{19}F has smaller negative Q_α value (-4.01 MeV) and ^{13}C has larger negative Q_α value (-10.64 MeV) than ^{18}O , ^{16}O , and ^{12}C projectiles; the values are tabulated in Table II. Thus, in order to understand the data presented in Fig. 4, the ICF fraction has been plotted in Fig. 6 as function of the

TABLE II. List of systems along with their entrance channel parameters: μ is the mass asymmetry, $Z_P Z_T$ the product of atomic numbers of interacting partners, Q_α^P the α - Q value of the projectile, and E_B^P the binding energy per nucleon of the projectile. The values of Q_α^P and E_B^P are in MeV.

System	μ	$Z_P Z_T$	Q_α^P	E_B^P	Ref.
$^{12}\text{C} + ^{103}\text{Rh}$	0.79130	270	-7.367	7.68	[64]
$^{20}\text{Ne} + ^{59}\text{Co}$	0.49367	270	-4.729	8.03	[62]
$^{12}\text{C} + ^{159}\text{Tb}$	0.85965	390	-7.367	7.68	[50]
$^{13}\text{C} + ^{159}\text{Tb}$	0.84884	390	-10.648	7.47	^a
$^{16}\text{O} + ^{115}\text{In}$	0.75573	392	-7.161	7.98	[56]
$^{12}\text{C} + ^{169}\text{Tm}$	0.86740	414	-7.367	7.68	[51]
$^{13}\text{C} + ^{169}\text{Tm}$	0.85714	414	-10.648	7.47	[54]
$^{12}\text{C} + ^{181}\text{Ta}$	0.87565	438	-7.367	7.68	[52]
$^{13}\text{C} + ^{181}\text{Ta}$	0.86598	438	-10.648	7.47	[52]
$^{16}\text{O} + ^{159}\text{Tb}$	0.81714	520	-7.161	7.98	[32]
$^{18}\text{O} + ^{159}\text{Tb}$	0.79661	520	-6.228	7.77	[58]
$^{16}\text{O} + ^{181}\text{Ta}$	0.83756	584	-7.161	7.98	[65]
$^{19}\text{F} + ^{159}\text{Tb}$	0.78652	585	-4.014	7.78	[34]

^aPresent work.

projectile's Q_α value for different projectiles on the same target at a constant E_{lab}/V_b .

It is evident from Fig. 6 that the percentage ICF fraction is more for the projectile with less negative Q_α value and that the ICF fraction significantly decreases as the Q_α value becomes more negative. For a projectile with a large negative Q_α value, more energy is required to break it into its constituents (less breakup probability) as compared to the projectile with relatively less negative Q_α value. Further, from this figure one may also notice that F_{ICF} does not depend linearly on the Q_α value of the projectile. The data presented in Fig. 6 show that the Q_α value is also an important entrance channel parameter, which dictates the breakup probability of the projectile and hence plays an important role in understanding the ICF reactions.

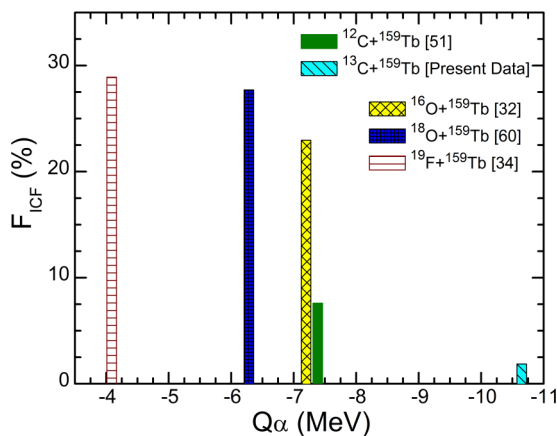


FIG. 6. A comparison of incomplete fusion fraction F_{ICF} in terms of the α - Q value of the projectile at a constant E_{lab}/V_b value for different projectiles on the same target, ^{159}Tb .

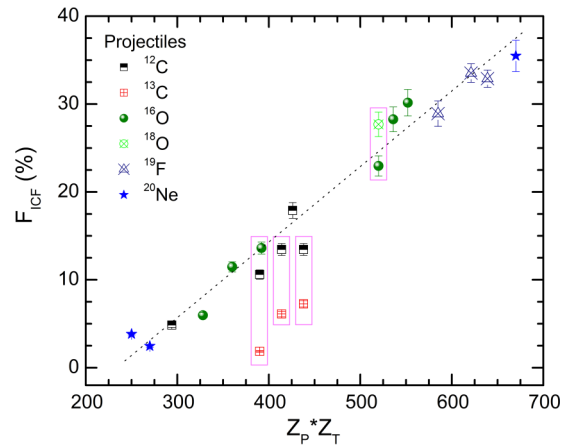


FIG. 7. The comparison of incomplete fusion fraction F_{ICF} values for various systems as a function of $Z_P Z_T$ at a constant E_{lab}/V_b value. The dashed line is drawn just to guide the eyes. Systems with same or almost same $Z_P Z_T$ values are marked by vertical boxes (see text for explanation).

4. ICF sensitivity to the Coulomb factor ($Z_P Z_T$)

From the previous subsections 2 and 3, it can be noticed that the ICF fraction depends on the projectile-target mass asymmetry, but increases with different gradients for different projectiles (see Fig. 4). On the other hand, according to the α - Q value systematics, the projectile's Q_α value determines the value of the F_{ICF} for different targets. Therefore, it may be inferred that these previous systematics are sensitive to the nature of either the projectile or the target nuclei. In another study the onset and strength of ICF fraction was also investigated in terms of the charge product of projectile and target (i.e., the product $Z_P Z_T$, where Z_P and Z_T are the atomic numbers of the projectile and target nuclei, respectively) [34]. The deduced ICF fraction for the presently studied system along with other projectile-target combinations have been plotted as a function of $Z_P Z_T$, at a constant E_{lab}/V_b , in Fig. 7. As can be seen from this figure, F_{ICF} does not follow any systematic trend; however, in general a linear growth in F_{ICF} may be seen when the charge product $Z_P Z_T$ increases. Hence, it is worthwhile to point out that, as the projectile approaches the target nucleus, the strength of the Coulomb interaction increases, resulting in the breakup of the projectile into its constituent fragments followed by fusion of one or more of the fragments. Thus, an increase in the value of $Z_P Z_T$ enhances the strength of Coulomb interaction, resulting in the larger magnitude of the breakup probability of the projectile.

Further, as can be seen from this figure, for the systems having same or almost same $Z_P Z_T$ values, marked by vertical boxes, the contribution of ICF is significantly different, which could not be explained on the basis of the recently proposed Coulomb-effect systematics [34]. A list of such systems is also given in Table II, with some of their entrance channel parameters. As a representative case, the F_{ICF} for a few systems with same or almost same $Z_P Z_T$ values are plotted

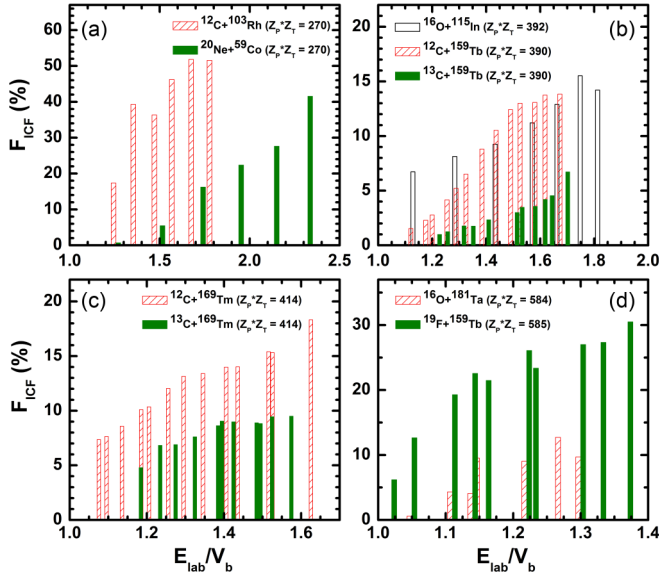


FIG. 8. Comparison of ICF fraction for different systems, at a constant $E_{\text{lab}}/V_b=1.35$, with same or almost same $Z_p Z_T$ values.

in Fig. 8, where it can be noticed that, in spite of having almost same the charge product, the values of F_{ICF} are significantly different at the entire studied energy range. For three systems, $^{16}\text{O} + ^{115}\text{In}$, $^{12}\text{C} + ^{159}\text{Tb}$, and $^{13}\text{C} + ^{159}\text{Tb}$, the values of $Z_p Z_T$ are almost equal; however, for the ^{16}O projectile the Q_α value is less negative, therefore it is expected to have a larger magnitude of incomplete fusion fraction than for the other two systems. This is confirmed by the observations of Fig. 8(b). Similar descriptions are valid for Figs. 8(c) and 8(d). Alternatively, the observations of Fig. 8 may be explained on the basis of Q_α values, i.e., whenever for two systems the $Z_p Z_T$ values are the same or almost same, then the magnitude of the ICF fraction is decided by the Q_α value of the projectile. However, the observed trend of F_{ICF} for the systems presented in Fig. 8(a) could not be explained by the above description. It may be noticed that the systems presented in Fig. 8(a) have smaller values of $Z_p Z_T$ ($=270$) than the other systems presented in Figs. 8(b)–8(d). The observed large ICF fractions for $^{12}\text{C} + ^{103}\text{Rh}$ may be explained by its larger mass asymmetry than the other system, rather than by the Q_α value of the projectile. This indicates that different entrance channel parameters may have different weights for different $Z_p Z_T$ values, but, to make the present observation more robust, a few more data sets at low $Z_p Z_T$ values are required. Further, the present analysis clearly shows that the Coulomb effect systematics alone is not able to explain the low-energy ICF reaction data and, of course, the Q_α value of the projectile or mass-asymmetry of the interacting partners may also be taken into consideration to understand the low-energy ICF-reaction dynamics. However, in order to reach to a final conclusion, more data at low energies, spanning a low to high mass region of target nuclei with different projectiles (i.e., covering a wide range of $Z_p Z_T$ values), is required.

IV. SUMMARY AND CONCLUSIONS

In the present work, the EFs of several radionuclides populated via CF and/or ICF in the $^{13}\text{C} + ^{159}\text{Tb}$ system have been measured in the energy range $1.01V_b$ to $1.68V_b$, and analyzed in the framework of compound nucleus theory, using the statistical model code PACE4. During the decay curve analysis for the identification of different reaction products, it has been found that some of the $p xn$ and αxn channels have contribution from precursor decay of a higher charge isobar. An attempt has been made to deduce the independent production cross section from cumulative and precursor decay contributions. The experimentally measured EFs of $xn/p xn$ channels have been found to agree reasonably well with the predictions of the statistical model code PACE4 done with level density parameter $a = A/8 \text{ MeV}^{-1}$, indicating their production via CF only. However, in the case of all α -emitting channels, a significant enhancement in the production cross sections has been observed as compared to the PACE4 predictions for the same set of parameters. This enhancement has been attributed to the contribution of ICF reactions. Although in the present work this estimation of ICF contribution is of course model dependent, the approach to deduce ICF contribution agree reasonably well with that of model independent approaches, such as the measurement of forward recoil ranges. Further, the satisfactory reproduction of CF contribution in the production of αxn -emitting channels deduced via recoil range distribution measurements, where CF and ICF contributions have been estimated separately by measuring full and partial linear momentum transfer components, clearly demonstrate the proper choice of PACE4 parameters used for the analysis, as well as the present method of deducing the ICF contribution using PACE4 predictions.

Further, from the analysis it has been observed that the ICF fraction strongly depends on the entrance channel parameters, such as incident beam energy, mass asymmetry of interacting partners, Q_α value of the projectile, and also the Coulomb-factor ($Z_p Z_T$). Clearly, from both the mass asymmetry and $Z_p Z_T$ systematics, it has been observed that the Q_α value is able to explain the observation of ICF for the same value of mass asymmetry or $Z_p Z_T$ of the interacting partners. In the present analysis, it may be concluded that a single parameter (i.e., mass asymmetry or $Z_p Z_T$ or Q_α value) is not able to explain, completely, the low energy incomplete fusion reactions. It is a combination of these parameters (or a parameter), which can incorporate all the gross features of interacting partners, that should be chosen. However, in order to achieve better understanding of the dependence of low-energy incomplete fusion reaction dynamics on various entrance channel parameters, more precise and diversified data (with the same compound nucleus or mass asymmetry or $Z_p Z_T$ values with different projectile-target combinations spanning a wide range of $Z_p Z_T$ values) is required. The new data will help us to reach conclusions about the transitions of different weights of entrance channel parameters and their effect on ICF reaction dynamics at low energies, and of course will help us to develop a universal systematics to understand the probability of involved reaction processes at such low energies.

ACKNOWLEDGMENTS

The authors thank to the Director, IUAC, New Delhi, India, for providing all the necessary facilities to carry out this work. The authors would also like to thank the Pelletron staff for providing the high quality beam during the experiment.

One of the authors (A.Y.) thank Dr. P. Sugathan and Mr. A. Jhingan, from IUAC, for their constant support and encouragement. A.Y. also thanks to the DST for providing support through the Young Scientist Scheme under startup research grant SB/FTP/PS-194/2013.

-
- [1] S. Hofmann *et al.*, *Euro. Phys. J. A* **32**, 251 (2007); **14**, 147 (2002).
- [2] V. I. Zagrebaev, *Nucl. Phys. A* **734**, 164 (2004).
- [3] L. Corradi *et al.*, *Nucl. Phys. A* **734**, 237 (2004).
- [4] Y. T. Oganessian *et al.*, *Nature (London)* **400**, 242 (1999), and the references therein.
- [5] M. Dasgupta *et al.*, *Nucl. Phys. A* **787**, 144 (2007); **734**, 148 (2004).
- [6] P. R. S. Gomes *et al.*, *Phys. Rev. C* **73**, 064606 (2006); *Phys. Lett. B* **601**, 20 (2004).
- [7] A. Diaz-Torres, D. J. Hinde, J. A. Tostevin, M. Dasgupta, and L. R. Gasques, *Phys. Rev. Lett.* **98**, 152701 (2007); *Phys. Rev. C* **65**, 024606 (2002).
- [8] E. Z. Buthelezi *et al.*, *Nucl. Phys. A* **734**, 553 (2004).
- [9] J. O. Newton *et al.*, *Phys. Lett. B* **586**, 219 (2004).
- [10] P. P. Singh *et al.*, *Phys. Lett. B* **671**, 20 (2009); *Phys. Rev. C* **80**, 064603 (2009); **78**, 017602 (2008).
- [11] C. Gerschel, *Nucl. Phys. A* **387**, 297 (1982).
- [12] M. Dasgupta *et al.*, *Phys. Rev. C* **70**, 024606 (2004).
- [13] L. F. Canto, R. Donangelo, L. M. de Matos, M. S. Hussein, and P. Lotti, *Phys. Rev. C* **58**, 1107 (1998).
- [14] U. Gupta *et al.*, *Nucl. Phys. A* **811**, 77 (2008).
- [15] U. Gupta *et al.*, *Phys. Rev. C* **80**, 024613 (2009).
- [16] D. P. Singh *et al.*, *Phys. Rev. C* **81**, 054607 (2010).
- [17] M. Lefort, *Rep. Prog. Phys.* **39**, 129 (1976).
- [18] H. C. Britt and A. R. Quinton, *Phys. Rev.* **124**, 877 (1961).
- [19] R. I. Badran *et al.*, *Eur. Phys. J. A* **12**, 317 (2001).
- [20] T. Udagawa and T. Tamura, *Phys. Rev. Lett.* **45**, 1311 (1980); *Phys. Lett. B* **116**, 311 (1982).
- [21] E. Takada, T. Shimoda, N. Takahashi, T. Yamaya, K. Nagatani, T. Udagawa, and T. Tamura, *Phys. Rev. C* **23**, 772 (1981).
- [22] J. Wilczynski *et al.*, *Phys. Rev. Lett.* **45**, 606 (1980); J. Wilczynski, *Nucl. Phys. A* **373**, 109 (1982).
- [23] M. Blann, *Phys. Rev. Lett.* **27**, 337 (1971).
- [24] J. P. Bondroff *et al.*, *Nucl. Phys. A* **333**, 285 (1980).
- [25] B. G. Harvey, *Phys. Lett. B* **130**, 373 (1983).
- [26] B. G. Harvey, *Nucl. Phys. A* **444**, 498 (1985).
- [27] A. Y. Abul-Magd, *Z. Phys. A* **298**, 143 (1980).
- [28] M. H. Simbel and A. Y. Abul-Magd, *Z. Phys. A* **294**, 277 (1980).
- [29] T. Inamura, M. Ishihara, T. Fukuda, T. Shimoda, and H. Hiruta, *Phys. Lett. B* **68**, 51 (1977); T. Inamura, T. Kojima, T. Nomura, T. Sugitate, and H. Utsunomiya, *ibid.* **84**, 71 (1982); T. Inamura, A. C. Kahler, D. R. Zolnowski, U. Garg, T. T. Sugihara, and M. Wakai, *Phys. Rev. C* **32**, 1539 (1985).
- [30] V. I. Zagrebaev, *Ann. Phys. (NY)* **197**, 33 (1990).
- [31] H. Morgenstern, W. Bohne, W. Galster, K. Grabisch, and A. Kyanowski, *Phys. Rev. Lett.* **52**, 1104 (1984); H. Morgenstern, W. Bohne, K. Grabisch, H. Lehr, and W. Stöffler, *Z. Phys. A* **313**, 39 (1983); H. Morgenstern, W. Bohne, K. Grabisch, D. G. Kovar, and H. Lehr, *Phys. Lett. B* **113**, 463 (1982).
- [32] P. P. Singh *et al.*, *Phys. Rev. C* **77**, 014607 (2008), and the references therein.
- [33] A. Yadav *et al.*, *Phys. Rev. C* **86**, 014603 (2012).
- [34] M. Shuaib *et al.*, *Phys. Rev. C* **94**, 014613 (2016).
- [35] A. Gavron, *Phys. Rev. C* **21**, 230 (1980).
- [36] O. B. Tarasov and D. Bazin, *Nucl. Instrum. Methods Phys. Res., Sect. B* **204**, 174 (2003).
- [37] N. G. Puttaswamy *et al.*, *Proc. DAE Symp.* **34B**, 405 (1991).
- [38] The Stopping and Range of Ions in Matter (SRIM) code, <http://www.srim.org/SRIM/SRIMLEGL.htm>
- [39] B. P. A. Kumar *et al.*, CANDLE–Collection and Analysis of Nuclear Data using Linux nEtworK, *Proc. DAE Symp.* **44B**, 390 (2001).
- [40] E. Browne and R. B. Firestone, *Table of Radioactive Isotopes* (Wiley, New York, 1986).
- [41] *Table of Isotopes*, 8th ed., edited by R. B. Firestone and V. S. Shirley (Wiley, New York, 1996).
- [42] V. R. Sharma *et al.*, *Phys. Rev. C* **84**, 014612 (2011).
- [43] S. F. Mughabghab, M. Divadeenam, and N. E. Holden, *Neutron Cross-Sections* (Academic, New York, 1981), Vol. 1, Part A, p. 89.
- [44] W. Hauser and H. Feshbach, *Phys. Rev.* **87**, 366 (1952).
- [45] A. Gilbert and A. G. W. Cameron, *Can. J. Phys.* **43**, 1446 (1965).
- [46] S. K. Kataria, V. S. Ramamurthy, and S. S. Kapoor, *Phys. Rev. C* **18**, 549 (1978); **19**, 297(E) (1979).
- [47] R. Bass, *Phys. Rev. Lett.* **39**, 265 (1977); *Nucl. Phys. A* **231**, 45 (1974).
- [48] R. D. Evans, *The Atomic Nucleus* (McGraw-Hill, New York, 1955).
- [49] S. Mukherjee *et al.*, *Int. J. Mod. Phys. E* **15**, 237 (2006).
- [50] A. Yadav *et al.*, *Phys. Rev. C* **85**, 034614 (2012).
- [51] P. P. Singh *et al.*, *J. Phys.: Conf. Ser.* **590**, 012031 (2015).
- [52] K. Surendra Babu *et al.*, *J. Phys. G: Nucl. Part. Phys.* **29**, 1011 (2003).
- [53] H. Kumar *et al.*, *Nucl. Phys. A* **960**, 53 (2017).
- [54] V. R. Sharma *et al.*, *Phys. Rev. C* **89**, 024608 (2014).
- [55] A. Sharma *et al.*, *J. Phys. G: Nucl. Part. Phys.* **25**, 2289 (1999).
- [56] K. Kumar *et al.*, *Phys. Rev. C* **89**, 054614 (2014).
- [57] K. Kumar *et al.*, *Phys. Rev. C* **87**, 044608 (2013).
- [58] A. Yadav *et al.*, *EPJ Web. Conf.* **117**, 08022 (2016).
- [59] M. Shuaib *et al.*, *Proc. DAE-BRNS Symp. Nucl. Phys.* **61**, 482 (2016).
- [60] A. V. Agarwal *et al.*, *Proc. DAE-BRNS Symp. Nucl. Phys.* **60**, 470 (2015).
- [61] R. Ali *et al.*, *J. Phys. G: Nucl. Part. Phys.* **37**, 115101 (2010).
- [62] D. Singh, R. Ali, M. A. Ansari, B. S. Tomar, M. H. Rashid, R. Guin, and S. K. Das, *Phys. Rev. C* **83**, 054604 (2011).
- [63] D. Singh *et al.*, *Nucl. Phys. A* **879**, 107 (2012).
- [64] B. Kumar *et al.*, *Phys. Rev. C* **59**, 2923 (1999).
- [65] D. P. Singh *et al.*, *Phys. Rev. C* **80**, 014601 (2009).